Investigation of the effects of borogypsum and silica fume on ceramic material's sintering and final properties

Çetin Öztürk [1,*], **Atilla Evcin** [2]

¹*Necmettin Erbakan University, Department of Old Tile Repairs, Konya, 42090, Turkiye*
²*Afyon Kocatepe University, Department of Material Science and Engineering, Afyonkarahisar, 03200, Turkiye*

ARTICLE INFO

ABSTRACT

The present study aims to investigate the utilization of two crucial industrial wastes, borogypsum, and silica fume, as the primary raw materials in the production of ceramic materials. For this purpose, different receipts were designed from boron waste (borogypsum) belonging to the Emet boric acid factory (Kütahya/Turkiye) and silica fume, which was taken from the electrometallurgy facilities (Antalya/Turkiye). Mixtures were prepared by mixing 90% waste material and 10% binder clay. The samples, prepared at different mixing ratios from both wastes, were pressed uniaxially at 10 MPa, and the shaped samples were then fired at 1000, 1050, 1100, and 1150°C. Physical and mechanical tests, as well as mineralogical and microstructural analyses, were carried out on the fired samples. The technical properties of the samples derived from the wastes were evaluated depending on the type of waste material and its usage amounts, and firing temperatures. It was found that using high borogypsum caused high firing loss, which negatively affects the material's dimensional stability. Moreover, it was determined that adding silica fume to borogypsum increased water absorption (WA) and porosity values, and decreased strength (BS) values accordingly. As a result, the water absorption and bending strength values obtained in the samples prepared from a mixture of 70% borogypsum and 20% silica fume sintered at 1050°C (WA:12.39%, BS:13.45 MPa) and 1100°C (WA:10.25%, BS:15.18 MPa) coincide with the technical specifications defined in EN ISO 10545-3 (WA>10%) and EN ISO 10545-4 (BS≥12 MPa) standards, so it can be considered possible to use as wall tiles.

1. Introduction

Industrialization, urbanization, and technological developments benefit human life, but they also bring along problems such as the reduction of natural resources over time and the generation of substantial amounts of waste. Protecting the environment from industrial wastes is very important for living creatures because the health of all living things and their environment are adversely affected by this waste and pollution. For this purpose, many scientists continue to explore alternative ways to recycle waste, protect living creatures and the environment, and limit the consumption of natural resources [1-6].

The production of engineering materials from waste materials and their possibilities of application for alternative purposes is an essential interest for engineers. Research on waste products will help solve many environmental problems and create new valuable findings in the engineering field. The production of ceramic materials is one of the possible ways to dispose of industrial wastes of organic and inorganic origin.

Since high-temperature heating >1000°C is required to produce ceramic materials, organics and volatile compounds in waste burn out and cause porosity in the structure. The porous structure dominates many properties of the material, such as lightness and insulation [1-2].

Boron minerals are Turkiye's most essential and strategic underground asset, with the world's largest boron deposits. Turkiye has approximately 73% of the world's boron reserves and the fist boron production capacity followed USA. Although there are many boron minerals in nature, colemanite, tincal, and ulexite are the boron minerals widely used industrially. These minerals are concentrated to produce boron compounds. Colemanite is reacted with sulfuric acid to produce boric acid. The main product of the reaction is boric acid, and gypsum is collected in the filters as a by-product of the boric acid production process [6-10]. Since the gypsum sludge contains about 3-6 % B_2O_3, it is called borogypsum (BG). Approximately $3.3×10^5$ tons per year of boric acid and $6.5-7×10^5$ tons per year of BG are produced in the factories located in Bandırma and

*Corresponding author: rcozturk@erbakan.edu.tr

Emet of Etimaden Inc. in Turkiye [4, 11]. BG discarded from the plant is stored in open areas. It is a valuable industrial waste for its B_2O_3 content, However, boron compounds in BG can be dissolved by rain, which can lead to soil and water pollution. Also, the high amount of boron content leads to economic loss [4, 5, 12].

Utilization of industrial wastes and by-products has become an exciting issue for scientists to investigate. There are several studies in the literature investigating mechanical, physical, and chemical properties of materials containing by-products and wastes such as phosphogypsum, tincal ore waste, colemanite ore waste, BG, etc., [7-10].

In recent years, BG has been widely used in various fields, such as material science, chemical, agricultural, and civil engineering applications, since it offers cost reduction, energy savings, and arguably superior products. Boncukcuoglu et al. [7] and Elbeyli et al. [17] investigated using BG instead of natural gypsum in cement mortar. It was reported that concrete containing BG exhibited better mechanical strength than one containing natural gypsum. Sevim and Tumen [18] and Alp et al. [19] noted that using BG as a set retarder in the cement industry might be possible. Kutuk-Sert and Kutuk [20] reported that it was possible to use BG as infill aggregate in asphalt concrete for road and highway construction. Abi [11] reported that it was possible to use 10% BG to increase mechanical strength in brick compositions. Demir and Keles [21] and Evcin and Yahsi Çelen [22] reported that BG was suitable for gamma-ray shielding material.

Silica fume (SF), also known as microsilica, is a sub-product of the foundry process in the elemental silicon and ferrosilicon alloys. This by-product, produced in the electric arc furnace during the production of metallurgical silicon and ferrosilicon alloys, is a fine, amorphous, spherical silica powder with a SiO_2 content of 85-95%. The fume produced at the furnace condenses into fine particles and is recovered from the process exhaust gases by classification and filtration. Submicron particle size (<1 μm), flabby nature (thus behaving like a fume or smoke when dispersed in the air), high surface area (~13.000-30.000 m^2/kg), spherical shape, and glassy structure make SF very reactive in hydrous and anhydrous reaction environments. The worldwide production of SF waste is estimated to be over 1 million tons annually. It is known that about 500,000 tons of this is in the USA, and 200,000 tons are in Norway. In Turkiye, SF productions from one ferrosilicon production plant are around 1,000 tonnes annually. Fumed silica is a compelling material due to its ultra-fineness and high silica content. It is mainly used as a mineral additive in materials such as cement and concrete to improve properties such as strength, permeability, corrosion resistance, and others [1, 23-27].

Most of the studies on the evaluation of waste are for the use of single waste material as a substitute in the composition of a product, and the amount of waste used is relatively low. The present study aims to investigate the possible use of BG and SF, which are two important industrial wastes, as primary raw materials in the production of ceramic materials. For this purpose, samples were produced from mixtures containing BG belonging to the Emet Boric Acid factory (Kütahya/Turkiye) and SF, which was taken from the Electrometallurgy facilities (Antalya/Turkiye) and these were fired at different temperatures. Physical and mechanical tests, as well as mineralogical and microstructural analyses, were carried out on the fired samples. Technical properties of the samples derived from the wastes were evaluated depending on the type of waste material and its usage amounts and firing temperatures.

2. Materials and Methods

2.1. Materials

In the present study, the fabrication of ceramic materials from two industrial wastes was investigated. The BG was provided by the Eti Mine Works and the representative wastes were taken from the outlet of the thickener unit at the plant in Emet (Turkiye). The particle size of BG is the fine (d_{10}) and coarse (d_{90}) fractions, and the median particle size (d_{50}) is 0.96, 3.4, and 14.88 μm. SF was provided by Etibank Ferro-Alloy Production. SF powders were taken from a plant in Antalya (Turkiye) and then used as received without any treatment being applied. The particle size of SF is the fine (d_{10}) and coarse (d_{90}) fractions, and the median particle size (d_{50}), 1, 6.6, and 16 μm, respectively. Chemical analyses of waste materials used were performed by using an X-ray fluorescence spectroscopy (XRF; Rigaku, ZSX Primus II, Japan). The chemical analysis of waste materials used in the bodies determined by the XRF method is presented in Table 1. The mineralogical phase analysis of both wastes was performed by an X-ray diffractometer (XRD; Bruker-D8 Advance, Germany), with CuKα radiation, to determine their present crystalline phases. The determined crystalline phases of waste materials used in the bodies are presented in Figure 1.
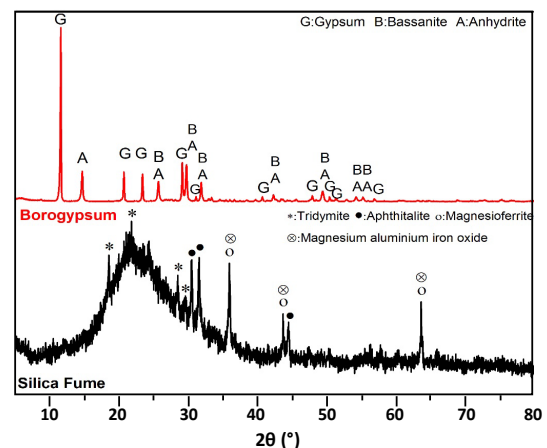

Figure 1. XRD analysis of waste materials as-received.

Table 1 show that BG consists mainly of calcium oxide (CaO), silicon oxide (SiO_2), and sulphur trioxide (SO_3) with relatively small and variable amounts of iron oxide (Fe_2O_3), magnesium oxide (MgO), aluminium oxide (Al_2O_3), and boron oxide (B_2O_3). Up to 20% ignition loss in the chemical composition of BG is remarkable. SF predominantly contains the SiO_2 component as well as relatively small and variable amounts of alkali and alkaline earth oxides, CaO, Al_2O_3, and Fe_2O_3. Its SiO_2 content is over 96%, as presented in Table 1. Kaolin has a typical aluminosilicate composition but, on the other hand, has a high loss on ignition (LOI).

Table 1. The chemical analysis of raw and waste materials used.

Composition (wt. %)	Borogypsum	Silica Fume	Kaolin
SiO_2	9.96	96.02	57.15
Al_2O_3	1.66	0.20	21.36
Na_2O	0.03	0.08	2.40
K_2O	0.92	0.08	1.24
CaO	36.70	1.40	0.55
MgO	2.33	-	0.80
Fe_2O_3	2.64	0.20	0.23
TiO_2	0.11	-	-
SO_3	22.57	0.21	-
SrO	2.27	-	-
B_2O_3	1.21	-	-
MnO	0.10	-	-
L.O.I.*	19.50	1.81	16.27

*L.O.I.: Loss on Ignition

According to the XRD patterns presented in Figure 1, it was determined that BG contains bassanite ($2CaSO_4 \cdot H_2O$) (Pdf: 00-047-0964) and anhydrite ($CaSO_4$) (Pdf: 01-076-6906) crystalline phases besides gypsum ($CaSO_4 \cdot 2H_2O$) (Pdf: 01-070-0982) mineral. On the other hand, in the XRD pattern of SF, it was observed that the structure was mainly amorphous, as expected. The crystalline phases detected in the SF structure were as follows; tridymite (SiO_2) (Pdf: 01-086-0681), aphthitalite (($K,Na)_3Na(SO_4)_2$) (Pdf: 00-020-0928), magnesioferrite ($MgFe_2O_4$) (Pdf: 01-0754392) and magnesium aluminium iron oxide ($MgAlFeO_4$) (Pdf: 01-071-4392).

2.2. Composition Design

In this study, five different recipes were designed in which the amount of BG and SF were varied, and the kaolin was kept constant. In the designed recipes, the amount of kaolin was kept constant at 10 wt. %, the amount of BG was systematically reduced, and the amount of SF was increased as much as the decreasing amount of BG as given in Table 2. The B_X-SF_Y formulation was used to symbolize the samples prepared from these designed recipes. Here 'B' stands for BG

while X stands for weight percentage of BG. The second index value, SF, was assigned to SF, and its weight percentage was encoded as Y. The mineralogical compositions and their chemical analysis of designed receipts are given in Tables 2 and 3, respectively.

Table 2. The chemical analysis of raw and waste materials used.

Sample Code	Borogypsum (wt. %)	Silica Fume (wt. %)	Kaolin (wt. %)
B90-SF0	90	0	10
B70-SF20	70	20	10
B45-SF45	45	45	10
B20-SF70	20	70	10
B0-SF90	0	90	10

Table 3. The chemical analysis of raw and waste materials used.

Composition (wt. %)	B90-SF10	B70-SF20	B45-SF45	B20-SF70	B0-SF90
SiO_2	14.68	31.89	53.41	74.92	92.13
Al_2O_3	3.63	3.34	2.97	2.61	2.32
Na_2O	0.27	0.28	0.29	0.30	0.31
K_2O	0.95	0.78	0.57	0.36	0.20
CaO	33.09	26.03	17.20	8.38	1.32
MgO	2.18	1.71	1.13	0.55	0.08
Fe_2O_3	2.40	1.91	1.30	0.69	0.20
TiO_2	0.10	0.08	0.05	0.02	0.00
SO_3	20.31	15.84	10.25	4.66	0.19
SrO	2.04	1.59	1.02	0.45	0.00
B_2O_3	1.09	0.85	0.54	0.24	0.00
MnO	0.09	0.07	0.05	0.02	0.00
L.O.I.*	19.18	15.64	11.22	6.79	3.26

*L.O.I.: Loss on Ignition

2.3. Sample Preparations

BG, taken from the facility as a cake, was first oven-dried and then crushed using a laboratory-type roll crusher with an opening of 1 mm, then sieved through a 250 μm sieve. The other raw materials were also first dried in an oven to keep the correct mixing ratio. The weighing of raw materials was performed using an electronic balance with a precision of 0.01 grams, according to the amounts given in Table 2. Mixtures of 500 grams were prepared to represent each recipe, as presented in Table 2. A dry grinding process was then performed using a planetary ball mill until a homogeneous mixture was obtained and until the particle size of the prepared mix decreased to the desired ratio. The grinding time required for the desired homogeneity and grain size was kept constant at 30 minutes for all series. The mixtures obtained in the desired grain size were sieved through a 100 μm sieve and dried in

an oven (Elektromag, Turkiye) at 110°C for 24 hours until they reached a constant weight. The dried mixtures were next hand-milled with an agate mortar and pestle. The ground mixtures were moisturized with sprayed water to between 5 and 5.5% moisture, and all mixtures were formed into granules. The granulated powders were shaped as prismatic (10×10×70 mm) test samples by a hydraulic press by applying 100 kg/cm². The test samples were dried in an oven at 110°C for 2 hours. The dried specimens were fired at 1000, 1050, 1100, and 1150°C in an electrically heated kiln at a heating rate of 5°C min⁻¹, holding the firing temperature for 1 hour.

3. Characterization

Test samples were prepared with five different recipes using two different types of industrial waste from the metallurgical and mining sectors. 10 samples from each group were measured to obtain reliable values for all tests performed to evaluate the physical properties of the test samples. The test results were made by taking the mean values of 10 measurements.

The linear shrinkage percentage of samples, shaped in rectangular prism geometry and then fired, was calculated by dividing the difference between the sample sizes measured before and after the firing stage by the value before firing and multiplying by 100. The water absorption values were determined by the ratio of the mass increase caused by water immersion, calculated by weighing the dry and water-saturated mass of the samples to the dry sample's weight. Bulk density values were determined by proportioning the weight of the relevant examples in the air to the mass difference between their water-saturated and water-suspended weights. Apparent porosity values were calculated by dividing the difference in mass caused by immersion of the samples in water to the value of the mass difference between the water-saturated and water-suspended weights of the relevant pieces and then multiplying by 100. The physical properties of fired samples (water absorption, porosity, firing shrinkage, etc.) were measured and evaluated according to TS EN ISO 10545-3 standards.

The bending strength (σ_F) of fired samples was measured according to EN ISO 10545-4 standards using a three-point bending test instrument (Shimadzu AG-IS, Japan). Five representative fired samples were used for the three-point bending test and the average fired strength values were calculated to represent the results better. The standard deviation was less than 1% of the average values.

The crystal structures of fired samples were characterized by an X-ray diffractometer (XRD; Bruker-D8 Advance) using Cu-Kα radiation (λ=1.5406 Å) scanning from 10° to 90° at a scanning rate of 2°/min, and the divergence and scattering slit widths were set at 0.30 mm. After a first visual inspection of the XRD patterns, the mineral spectral search and match

confirmation were analysed. Basic data processing and phase identification were performed by Bruker EVA software and the ICDD PDF-2 database.

Using scanning electron microscopy (SEM; Leo 1430 VP, Germany), the microstructure of fired samples has been examined in terms of formed phases, porosity, etc. During the observation, secondary electron images (SEI) at different magnifications of the fractured surface of the fired sample were used. The particle sizes of grains and pore sizes in microstructure were manually measured using the scale bar on the SEM micrographs. At least five measurements for each sample were performed. EDX (Energy Dispersive X-ray) analyses were also performed to identify crystalline phases.

4. Results and Discussion

4.1. Physical and Mechanical Properties of the Material Produced from Wastes

The results of characterization work on fired samples of encoded B90-SF10, B70-SF20, B45-SF45, B20-SF70, and B0-SF90 are given in Table 4. The linear shrinkage (LS), water absorption (WA), apparent porosity (AP), bulk density (BD), and bending strength (BS) values of fired samples are presented in Table 4, depending on the change in both firing temperature and amount of BG.

The effect of firing temperature and BG amount on the linear shrinkage of the samples fired at different temperatures is shown in Figure 2. It is seen that the linear shrinkage values of the fired samples gradually decreased with the decreasing BG amount at all temperatures. This decreasing trend in linear shrinkage values coincides with the LOI values of the compositions presented in Table 3. As seen in Table 3, as the amount of BG in the recipes decreases, the fire loss values decrease. Since SF has a much lower LOI values than BG (Table 1) and the replacement of BG by SF reduces the LOI values of the mixture.

Reducing linear shrinkage values with SF addition is considered favourable for the dimensional stability of material during firing. Because the high shrinkage
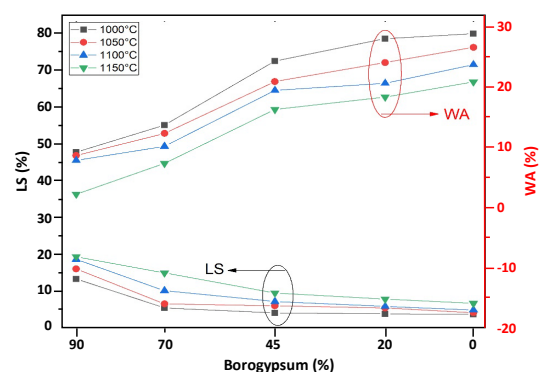

Figure 2. Linear shrinkage (LS) and water absorption (WA) in the samples as a function of firing temperature.

Table 4. Some properties of samples prepared from borogypsum and silica fume wastes.

Temperature (ºC)	Borogypsum (%)	LS (%)	WA (%)	AP (%)	BD (g/cm³)	BS (MPa)
1000	90	13.54	9.29	18.57	1.99	13.27
	70	5.68	13.77	25.93	1.72	11.36
	45	4.32	24.39	35.61	1.60	9.84
	20	4.05	28.10	39.04	1.55	7.25
	0	3.96	28.93	39.30	1.35	4.66
1050	90	16.23	8.72	17.78	2.04	16.06
	70	6.75	12.39	22.33	1.78	13.48
	45	6.22	20.99	33.47	1.66	12.09
	20	5.67	24.13	39.25	1.64	9.86
	0	4.38	26.66	39.34	1.57	6.18
1100	90	18.83	7.92	16.91	2.13	19.23
	70	10.34	10.25	20.52	1.83	15.18
	45	7.41	19.53	32.10	1.74	13.26
	20	6.08	20.71	39.34	1.68	11.07
	0	5.13	23.79	40.06	1.62	9.64
1150	90	19.57	2.32	9.64	2.44	23.64
	70	15.14	7.42	17.53	2.24	16.41
	45	9.72	16.36	24.67	1.84	14.71
	20	8.06	18.42	39.95	1.71	11.89
	0	6.90	20.93	40.27	1.65	10.15

results in a lack of dimensional stability in materials, which leads to an important loss of end-product quality (deformation, size mismatch, etc.), as well as problems in the application of materials (tiling, brick-laying, etc.). Producing materials free of dimensional defects is required using appropriate control of the body composition and temperature distribution in the firing process. The most important precaution that can be taken for body composition is to avoid using the raw materials in high amounts that can cause high shrinkage.

From this point of view, the high shrinkage values obtained in the series with the highest BG content (B90-SF0) are considered not suitable for the dimensional stability of the final product. On the other hand, it can be observed that there is a severe decrease in shrinkage values with the incorporation of SF in their body compositions (Figure 2). This situation is related to the fact that silica preserves its dimensional stability at firing temperatures reducing the distortion and shrinkage of the bodies, as expressed in many previous studies [28-31].

As indicated in Table 4, the water absorption values measured in the samples prepared using waste materials are above 10% in all samples except for the samples with 90% BG content for 1000, 1050, and 1100°C temperatures and 70% and 90% BG content for 1150°C. SF addition increased the values of the water absorption of the samples at all firing temperatures (Figure 2). However, at all firing temperatures,

samples containing the maximum amount of SF have at least 15% higher water absorption values than those without SF. This observation can be attributed to the decreasing shrinkage and low packing density induced by the use of SF, resulting in increased water absorption values.

Water absorption is an essential factor in ceramic materials' durability and liquid permeability. Water absorption is directly proportional to apparent porosity [2]. Therefore, similar trends were observed in water absorption and apparent porosity (Figure 3).

As presented in Table 4, the lowest bulk density value which was to be 1.35 g/cm³ was obtained in the sample that did not have BG and was fired at 1000°C,
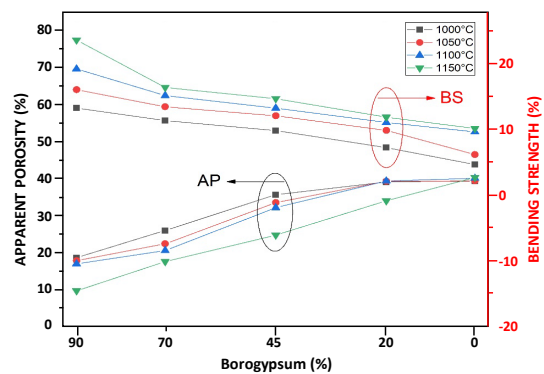

Figure 3. Apparent porosity (AP) and bending strength (BS) in the samples as a function of firing temperature.

while the highest bulk density value of 2.44 g/cm³ was obtained in the sample that did not have SF and was fired at 1150°C. The bulk density values of the bodies increased with the increase in temperature. This can be associated with the reduction of porosity in number and size. On the other hand, with the increase of SF, the bulk density values of the bodies decreased. This observation can be attributed to the reduced shrinkage and lower packing density caused by the use of SF, as discussed in the water absorption results.

Due to the increase in the degree of sintering, the size and number of internal pores in the material decreases, and the degree of packing increases, resulting in higher bulk density values. Conversely, under poor sintering conditions, porosity increases, and the material becomes less dense; as a result, the bulk density of the body is reduced, resulting in an underdeveloped microstructure. As a result, the use of SF in waste-containing bodies resulted in an increase in porosity, a reduction in firing shrinkage, and a decrease in bulk density values as a result of these, which is an indication that the sintering process is negatively affected.

It can be seen that the apparent porosity values presented in Table 4 are below 20% in all samples without SF and above 20% in samples containing SF, except B70SF20. Parallel to the increase in SF usage, AP values increased in all samples (Figure 3). On the other hand, except for the series in which SF is used at the amount of 70 and 90%, it can be seen that the AP values of the samples decrease with increasing temperature in the other series. On the contrary, it was observed that AP increased with the increase in temperature in the series in which SF was used at a high rate (>70%). High apparent porosity (AP) and associated high water absorption (WA) result in reduced material mechanical strength. When evaluated within this framework, the addition of SF at increasing rates to BG adversely affected the mechanical strength of the material produced from these wastes.

As presented in Table 4, the lowest bending strength value to be 4.66 MPa was obtained in the sample that did not have BG and was fired at 1000°C, while the highest bending strength value to be 23.64 was obtained in the sample that did not have SF and was fired at 1150°C. The bending strength values of the bodies increased with the increase in temperature (Figure 3). This can be attributed to a decrease in porosity in number and size, as discussed earlier in the evaluation of bulk density results. On the other hand, with the increase of SF, the bending strength values of the bodies decreased. This observation can also be attributed to the reduced shrinkage and lower packing density caused by the use of SF, as discussed in the water absorption and bulk density results.

4.2. Microstructural Evaluation

After the determination of the physical and mechanical properties, the samples belonging to the B70SF20

coded series, sintered at 1000 and 1100°C were selected for phase analysis, since they have low LS and WA, and high BS values. The XRD analysis of the sample (B70SF20) of materials produced from the industrial wastes is given in Figure 4. There was no remarkable change in the phase structure of samples with the increasing firing temperature, and it was found that the phase structure of the samples included similar phases, i.e., calcium sulphate ($Ca(SO_4)_2$), calcium silicate (Ca_2O_4Si), and augite ($(Si, Al)_2O_6$). As the difference in XRD patterns drawn for two different temperatures; in the sample fired at 1100°C, a cristobalite peak was detected at 2θ:21.8° in the XRD pattern, while an increase in the number of augite peaks was detected.
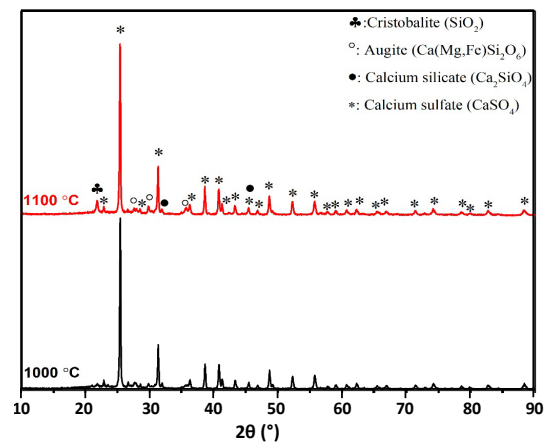

Figure 4. XRD analysis patterns of fired samples at two different temperatures.

According to XRD analysis, it can be seen that the main phase forming the microstructure of the waste originating material consists of calcium sulphate from BG. In the composition (B70SF20), where 70% BG and 20% SF are used, it can be understood that calcium silicate and augite compounds are formed depending on the reactions between BG and SF.

The secondary electron images (SEI) taken from the fractured surfaces of the sample belonging to the bodies incorporated 20% SF (B70SF20) and which were fired at 1100°C are given in Figure 5. From the SEI images presented in Figure 5, the presence of crystalline phases such as calcium sulphate and calcium silicate, and also glassy phase in the microstructure of the waste-based material was determined. In SEM figures, letters indicate CSu: calcium sulphate, CSi: calcium silicate, G: glassy phase, P: porosity.

In the micrographs taken at low magnification of the sample examined in the SEM analysis, it can be understood that the general microstructure image is homogeneous and dense but also contains pores. In the micrographs taken at high magnifications, it can be seen that the grains of calcium sulphate, which are 1-3 μm in size, are both embedded in the glass phase and the form of independent grains outside the glass

phase. In addition, needle-like calcium silicate crystals showing an aspect ratio in the 10:1 interval (~1 µm long and ~0.1 µm wide) were also observed in the micrograph taken at the highest magnification of the sample, which was exposed to microstructure examination. On the other hand, it has been determined that the majority of the pores in the microstructure are not spherical but hollow and pitted, and the largest pores are around 1-2 µm.

In this study, which was carried out to investigate the effects of BG and SF on the sintering and final properties of ceramic materials, heat microscopy analysis of SF was carried out to explain its effect on the sintering, microstructural development, and technical properties.

The melting behaviour of SF was determined by the Optonom Scientific Instruments brand heat microscope (Optonom Scientific Instruments, Turkiye) in Figure 6. By using the heat microscope, the physical changes of the sample with the increase in temperature (sintering temperature, softening temperature, sphere temperature, hemisphere temperature, yield temperature) and the temperatures at which these changes occur can be determined. It is seen that the sintering temperature, softening temperature, hemisphere temperature and yield temperature determined by the heat microscope of SF are 933, 1032, 1196 and 1199°C, respectively.
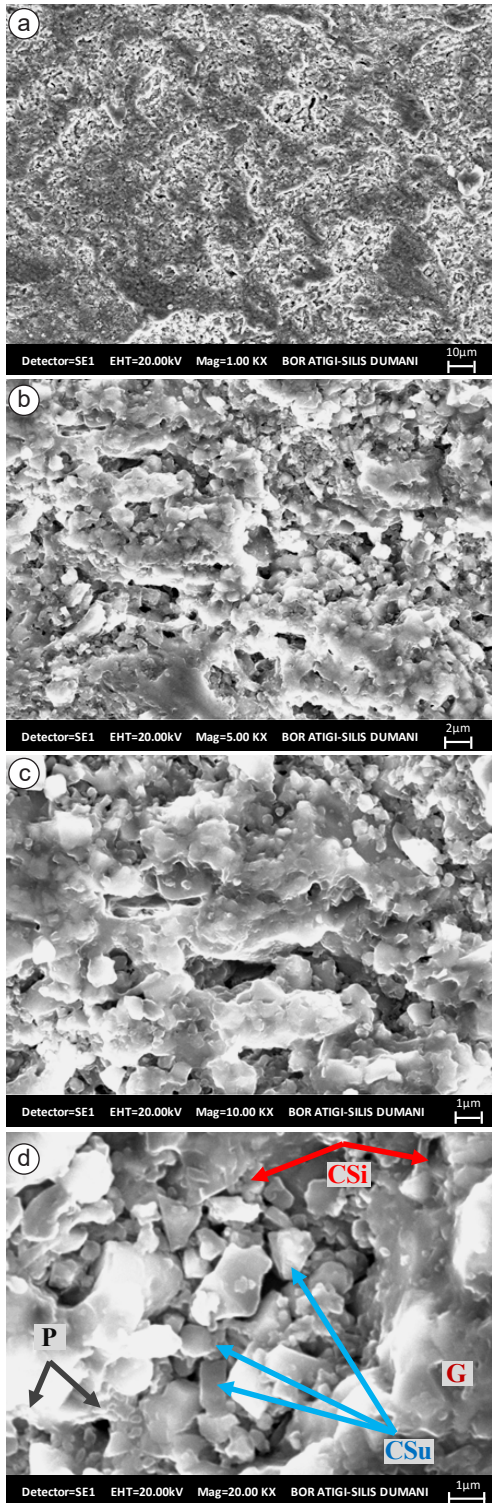

Figure 5. Secondary electron image of B70SF20 at different magnifications; (a) 1000X, (b) 5000X, (c) 10000X, and (d) 20000X.
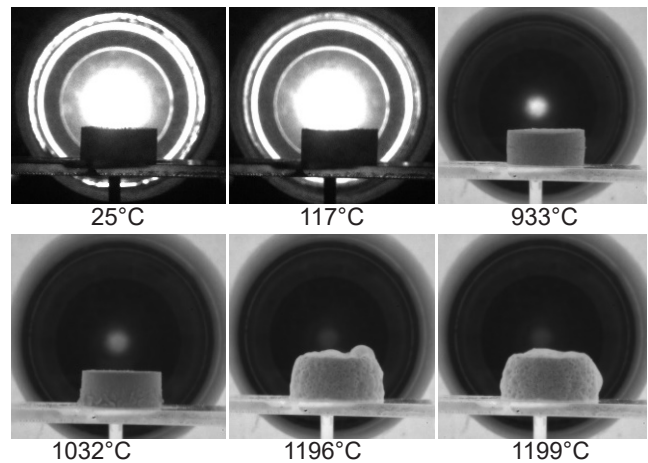

Figure 6. Heat microscope analysis of silica fume.

According to the results of the physical and mechanical properties, the B70SF20 coded samples, which were determined to have the best properties, during the sintering process at 1000-1150°C, the SF did not completely pass into the molten phase (because it began to soften at 1032°C and flow at about 1200°C). It is thought that this molten phase has a high viscosity. In the SEM micrograph of the sample sintered at 1100°C, code B70SF20, it is understood that the partial molten phase formed from SF partially encloses the grains of the other components, while the parts that the liquid phase does not wrap remain in the structure as open porosity. Additionally, it can be understood that the gas releases originating from BG and kaolin, which have higher heating loss than SF, do not cause foaming in this high-viscosity melt phase. On the other hand, although gas escape is provided from the remaining (not surrounded by amorphous) openings, it can be said that some of them are trapped in the glassy phase (as closed porosity) due to the increase in porosity.

5. Conclusion

From the two industrial wastes used, it can be understood that the high ignition loss of BG will cause more firing shrinkage in the samples to be produced entirely using BG, thus posing a problem in terms of material dimensional stability. For this reason, it can be understood that using additional raw materials to reduce LOI originating from BG is required. On the other hand, it was determined that with the increase of SF addition to BG, the water absorption and porosity values increased, and the strength values decreased accordingly. The effects on the material properties of usage of both BG and SF in the composition together or individually were evaluated. It can be understood that the optimum composition should be adjusted by using a minimum amount of SF that will not adversely affect the technical properties and in an amount that will reduce the LOI originating from BG and thus shrinkage. In this context, it has been shown that the technical properties obtained in the samples prepared from a mixture of 70% BG and 20% SF can be considered wall tile since they coincide with the water absorption and strength values defined in the EN ISO 10545-3 (WA%>10) and EN ISO 10545-4 (BS≥12 MPa) standards, respectively.

As a result, when all the technical properties are evaluated, it can be concluded that the usage of BG and SF for producing wall tiles materials will be possible through optimizations in body composition and/or operational conditions.

References

[1] Baspinar, S., Demir, I. & Orhan M. (2010). Utilization potential of SF in fired clay bricks. *Waste Management & Research*, *28*, 149-157.

[2] Bahtli, T., & Erdem Y. (2022). The use of foundry waste sand from investment casting in the production of porcelain tiles. *Ceramics International*, *48*(19A), 27967-27972.

[3] Zaimoglu, S. A. (2011). Engineering properties of sand stabilised with borogypsum. *Proceedings of the Institution of Civil Engineers-Geotechnical Engineering*, *164*, 277-282.

[4] Simsek, H. M., Guliyev, R., & Bese, A. V. (2018). Dissolution kinetics of borogypsum in di-ammonium hydrogen phosphate solutions. *International Journal of Hydrogen Energy*, *43*(44), 20262-20270.

[5] Elbeyli, I. Y., & Piskin, S. (2004). Kinetic study of the thermal dehydration of borogypsum. *Journal of Hazardous Materials*, *116*(1-2), 111-117.

[6] Kunt, K, Dur, F., Yildirim, M., & Derun, E. M. (2017). Effect of chemical admixtures on borogypsum containing cement mortar. *Main Group Chemistry*, *16*(4), 227-239.

[7] Boncukcuoglu, R., Yilmaz, M. T., Kocakerim, M. M., & Tosunoglu, V. (2002). Utilization of borogypsum as set retarder in Portland cement production. *Cement and Concrete Research*, *32*(3), 471-475.

[8] Ozdemir, M., & Ozturk, N. U. (2003). Utilization of clay wastes containing boron as cement additives. *Cement and Concrete Research*, *33*(10), 1659-1661.

[9] Sevim, U. K., Ozturk, M., Onturk, S., & Bankir, M. B. (2019). Utilization of boron waste borogypsum in mortar. *Journal of Building Engineering*, *22*, 496-503.

[10] Ozturk, M., Sevim, U. K., Akgol, O., Unal, E., & Karaaslan, K. (2020). Investigation of the mechanic, electromagnetic characteristics and shielding effectiveness of concrete with boron ores and boron containing wastes. *Construction and Building Materials*, *252*, 119058, 1-11.

[11] Abi, C. B. E. (2014). Effect of borogypsum on brick properties. *Construction and Building Materials*, *59*, 195-203.

[12] Delfini, M., Ferrini, M., Manni, A., Massacci, P., & Piga, L. (2003). Arsenic leaching by Na2S to decontaminate tailings coming from colemanite processing. *Minerals Engineering*, *16*, 45-50.

[13] Holanda, F. C., Schmidt, H., & Quarcioni, V. A. (2017). Influence of phosphorus from phosphogypsum on the initial hydration of Portland cement in the presence of superplasticizers. *Cement and Concrete Composites*, *83*, 384-393.

[14] Abali, Y., Bayca, S. U., & Targan, S. (2006). Evaluation of blends tincal waste, volcanic tuff, bentonite and fly ash for use as a cement admixture. *Journal of Hazardous Materials*, *131*(1-3), 126-130.

[15] Kaman, D. O., Koroglu, L., Ayas, E., & Guney, Y. (2017). The effect of heat-treated boron derivative waste at 600°C on the mechanical and microstructural properties of cement mortar. *Construction and Building Materials*, *154*, 743-751.

[16] Sevim, U. K. (2011). Colemanite ore waste concrete with low shrinkage and high split tensile strength. *Materials and Structures*, *44*, 187-193.

[17] Elbeyli, I. Y., Derun, E. M., Gulen, J., & Piskin S. (2003). Thermal analysis of borogypsum and its effects on the physical properties of Portland cement. *Cement Concrete Research*, *33*,1729-1735.

[18] Sevim U. K., & Tumen Y. (2013). Strength and fresh properties of borogypsum concrete. *Construct Build Mater*, *48*, 342-347.

[19] Alp I., Deveci, H., Sungun, Y. H., Yazici, E. Y., Savas, M., & Demirci, S. (2009). Leachable characteristics of arsenical borogypsum wastes and their potential use in cement production. *Environmental Science & Technology*, *43*, 6939-6943.

[20] Kutuk-Sert T., & Kutuk, S. (2013). Physical and marshall properties of borogypsum used as filler aggregate in asphalt concrete. *Journal of Materials in Civil Engineering*, *25*(2), 266-273.

[21] Demir, D, & Keles, G. (2006). Radiation transmission of concrete including boron waste for 59.54 and 80.99 keV gamma rays. *Nuclear Instruments and Methods in Physics Research Section B: Beam Interactions with Materials and Atoms*, *245(2)*, 501-504.

[22] Celen, Y. Y., & Evcin, A. (2020). Synthesis and characterizations of magnetite-borogypsum for radiation shielding. *Emerging Materials Research*, *9*(3), 1-7.

[23] Muller, A. C. A., Scrivener, K. L., Skibsted, J., Gajewicz, A. M., & McDonald, P. J. (2015). Influence of SF on the microstructure of cement pastes: new insights from H NMR relaxometry. *Cement and Concrete Research*, *74*, 116-125.

[24] Sanjuán, M. A., Argiz, C., Gálvez, J. C., & Moragues, A. (2015). Effect of SF fineness on the improvement of Portland cement strength performance. *Construction and Building Materials*, *96*, 55-64.

[25] Siddique, R. (2011). Utilization of SF in concrete: review of hardened properties. *Resources, Conservation and Recycling*, *55*, 923-932.

[26] Khan, M. I., & Siddique, R. (2011). Utilization of SF in concrete: review of durability properties. *Resources, Conservation and Recycling*, *57*, 30-35.

[27] Ávalos-Rendón, T. L., Chelala, E. A. P., Mendoza Escobedo, C. J., Figueroa, I. A., Lara ,V. H., & Palacios-Romero, L. M. (2018). Synthesis of belite cements at low temperature from SF and natural commercial zeolite. *Materials Science and Engineering: B*, *229*, 79-85.

[28] Ozturk, C., Akpınar, S., & Tığ, M. (2022). Effect of calcined colemanite addition on properties of porcelain tile. *Journal of the Australian Ceramic Society*, *58*, 321-331.

[29] Ozturk, C., Akpınar, S., & Tarhan, M. (2021). Investigation of the usability of Sille stone as additive in floor tiles. *Journal of the Australian Ceramic Society*, *57*(2), 567-577.

[30] Ozdemir, Y., Akpınar, S., & Evcin, A. (2017). Effect of calcined colemanite additions on properties of hard porcelain body. *Ceramics International*, *43*(11), 8364-8371.

[31] Turkmen, O., Kucuk, A., & Akpinar, S. (2015). Effect of wollastonite addition on sintering of hard porcelain. *Ceramics International*, *41*(4), 5505-5512.